JOURNAL OF THERMOPHYSICS AND HEAT TRANSFER
Vol. 23, No. 4, October–December 2009

Nondestructive Evaluation of Surface Defects Using Scanning Infrared Thermography

C. Dalton,* B. Olson,† and F. C. Lai‡
University of Oklahoma, Norman, Oklahoma 73019

DOI: 10.2514/1.44021

Nondestructive evaluation techniques are important for the aircraft industry and infrared scanning systems have the potential to analyze materials and parts, quickly, accurately, and at a reduced cost compared with other systems. This technique has been developed to create an interface using commercial software packages. New hardware components have been designed to work in concert with specially developed analytical models to treat surfaces with changing emissivity and uniformly finished surfaces such as those used in traditional infrared scanning systems. The current scanning system has been tested using crack defects in thin metal sheets with a variety of surface finishes and defect geometries. The system has been successful at detecting defects on coated surfaces on which cracks were oriented parallel to the heating element and at suboptimal angles. However, the system has only been marginally successful at removing artifacts of reflected radiation from the thermographic images, making temperature correction and crack detection difficult.

Nomenclature

J	=	radiosity
T	=	temperature
α	=	absorptivity
ε	=	emissivity
ρ	=	reflectivity
Σ	=	Stefan–Boltzmann constant
τ	=	transmissivity

Subscripts

actual	=	true value
amb	=	ambient
cam	=	camera
meas	=	measured quantity
ref	=	reflected quantity

I. Introduction

NONDESTRUCTIVE evaluation (NDE) is a method in which materials or parts can be evaluated without damaging the part, such that it can be reused [1]. This saves time and money by allowing data to be collected on a specific device, part, or material instead of using general data from published references. In addition, the first signs of failures can be seen before harmful damage is made, thus avoiding the dangerous consequences a failure can bring. NDE is used frequently in situations in which systems undergo cyclic or repeated stresses. These stresses are below the ultimate failure limits, but over time, these smaller stresses can eventually build to fracture. Therefore, it is imperative to scan systems, parts, and materials for these early defects that can ultimately lead to disaster.

There are numerous nondestructive methods currently available for detecting defects in parts or materials, such as x-ray imaging, eddy current testing, and acoustic methods that are available in both ultrasonic and subsonic frequencies. Although each of these techniques has merit and is successful in certain cases, there are situations in which the best technique is still visual hand inspection, in which trained personnel carefully scan parts and materials for dangerous areas. Unsurprisingly, this can take an unusual amount of time, and so there are searches underway to find a system or method that allows for high defect resolution as well as faster analysis. Infrared scanning is one promising method that could potentially meet these requirements.

Infrared scanning systems are not new; they have been used in numerous applications in biology, astronomy, and even the military. Even in basic infrared evaluation, surface temperature is the valued information that is used to infer characteristics of the given item. However, infrared scanning systems can add a new dimension to their capabilities when principles of heat transfer are considered, particularly Fourier's law of heat conduction. Fourier's law states that the amount of heat transfer through a material is based on three factors: temperature gradient, cross-sectional area, and thermal conductivity. Therefore, if the amount of heat transfer is held constant, changes in the thermal conductivity or cross-sectional area directly affect the temperature gradient within the material. As a heat flux passes through a pure substance, it will create a smooth temperature gradient based on the material's thermal conductivity and cross-sectional area. However, if either of the properties varies through a particular part or piece, the temperature gradient will veer from the expected distribution and display anomalies. Although these anomalies might be difficult to detect using physical contact temperature measurement devices, they become very easy to see when using an infrared scanning device [2,3]. From this point, one only has to identify the locations of the temperature anomalies and perform closer examinations to determine the reason for the shift.

The idea of using infrared scanning systems in conjunction with prescribed heat transfer to detect anomalies has been studied for several years [4–11]. Up to this point, most of the systems are purely laboratory variety, in which they are not adapted to real-world applications. Presently, many of these systems are still too complex and the technology too involved to be used by most laymen. There are many opportunities to not only adapt a system to fit more applications, but also to simplify the process to allow for easier acquisition and data processing. The system presented within is an attempt to tackle one particular application: the scanning of airplane skin for crack defects. In addition to this particular application for the aircraft industry, the system created has also been built with a much simpler user interface that will allow for varying levels of analysis complexity that can be contoured to the changing skill level of the user. As well as simplifying the interface, another innovation presented within is the ability to scan materials and parts regardless of their surface coating.

Received 25 February 2009; revision received 22 May 2009; accepted for publication 28 May 2009.

*Graduate Research Assistant, School of Aerospace and Mechanical Engineering.

†Assistant Professor, School of Aerospace and Mechanical Engineering; currently ITT Corporation, Rochester, NY.

‡Associate Professor School of Aerospace and Mechanical Engineering. Associate Fellow AIAA.

This system has been developed with the ability to analyze parts or materials with low or variable emissivity. Because infrared camera systems continue to become less expensive than other scanning options, it is our hope that this can be developed into a simple, quick, and, above all, inexpensive method to carry out nondestructive evaluation and assist in preventative maintenance. Thus, the objectives of the present study can be summarized next:

1) Create an infrared scanning system, with accompanying software, that allows for quick, simple analysis of thermal images.

2) Detect crack defects in a variety of environments.

3) Develop a system that can analyze surfaces with low or variable emissivity.

II. Experimental Apparatus and Procedure

The system's overall function is to detect thermal anomalies within a material sample by recording the surface temperature changes over time using an infrared camera. As shown in Fig. 1, the temperature of the material is raised by concentrating the radiative output of a commercial halogen light bulb at the surface and allowing the heat to dissipate through the material. As the heat permeates the material, it alters the surface temperature, which can be recorded by the infrared camera.

The camera, heating lamp, and other hardware are mounted to a plywood shelf, which is mounted on a pair of commercially available drawer slides. This allows the scanning equipment to translate in a direction parallel to the anticipated direction of the applied heat flux. The upper shelf of the test rig also has the ability to be adjusted vertically to allow for a change in camera view by bringing the sample closer to the scanning equipment.

Figure 2 shows a side view and bottom view of the heating element and radiation shielding. The heat source used is a 500 W halogen bulb with a stainless steel reflector placed around it. The purpose of the reflector is to not only redirect some of the light and heat toward the sample, but also to prevent unwanted heating to the adjacent equipment, particularly the infrared camera. In addition to the bulb reflector, there is a series of radiation shields placed between the heat source and the camera. The shielding also serves two purposes: first, to block the intense heat emanating from the halogen lamp from damaging the infrared camera, and second, to block any radiation from reflecting off the sample being scanned and skewing the thermographic image received by the camera.

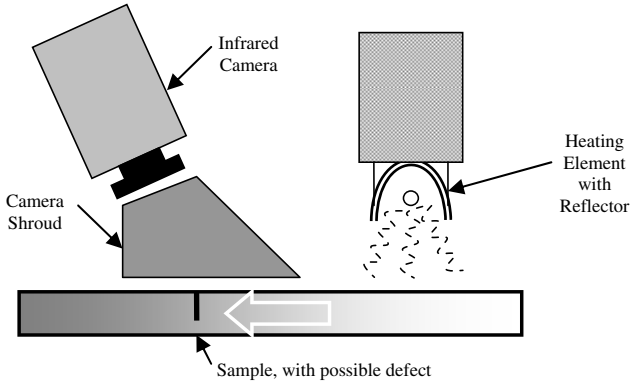

Fig. 1 Schematic of the proposed scanning system.

The camera used in this application is the FLIR Thermovision A20M. The camera produces images with a resolution of 320 by 240 pixels at a maximum rate of 60 frames per second [12]. The camera can detect temperatures within the range of −20 to 250°C with a minimum temperature resolution of 0.1°C and reported accuracy of ±2% [12]. In addition to the camera's ability to upload data to a computer, the camera itself has an onboard software package that allows for detailed analysis with numerous adjustable functions, including spot temperatures, boxes, minimum/maximum temperatures, and temperature alarms to fine-tune data collection [12]. The camera captures the thermographic images by measuring the amount of radiation received (radiosity) through the lens from each point within the camera's view angle, which is reported to be 45 deg horizontally and 35 deg vertically [12]. However, to accurately determine the temperature value, the camera takes into account several environmental parameters. For precise measurements to be made, the distance to and emissivity ε_{cam} of the target must be known, as well as the temperatures of the ambient environment and the air between the camera and the target surface (T_{amb}). Equation (1) shows the mathematical formula used to calculate the true temperature of the surface in question (T_{meas}):

$$\varepsilon_{\text{cam}}\sigma T_{\text{meas}}^4 + (1 - \varepsilon_{\text{cam}})\sigma T_{\text{amb}}^4 = J_{\text{cam}} \tag{1}$$

The radiation received by the camera (J_{cam}) comes from three sources: the emitted radiation of the surface being measured, the reflected radiation from the same surface, and the attenuation of the fluid between them. Only the surface emitted radiation provides the true temperature of the source, and so the other two radiation components must be eliminated or at least accounted for to obtain a true temperature profile. For the present study, the distance between the camera and the sample is sufficiently small that air attenuation effects are negligible.

Although the resolution and sensitivity of the infrared (IR) camera itself is quite good, the operating system provided is not capable of sophisticated data manipulation or correction, such as in the case of variable-emissivity surfaces. To maximize the camera's utility, it is best to remotely connect the camera to a computer program that allows direct control of camera settings as well as automated data collection. Although the camera can be controlled quite easily by remote access, the camera still has difficulty with low- and variable-emissivity surfaces. The onboard software will take into account a value of emissivity specified by the user, but this value cannot be changed with any speed. Therefore, it would not be possible to continually correct emissivity if a surface was being scanned that had a variation of emissivity.

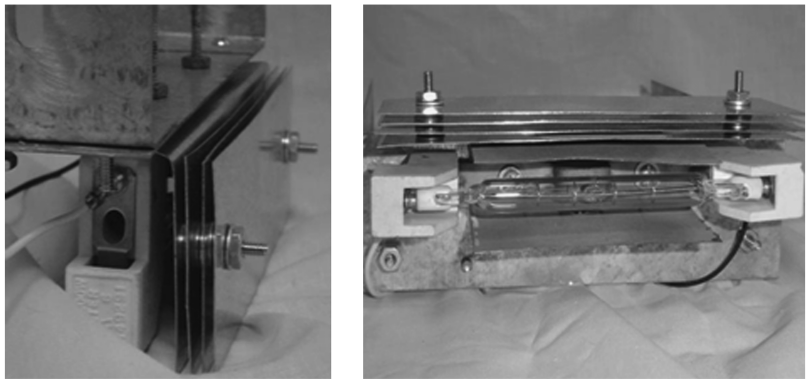

a) **b)**

Fig. 2 Heating element and radiation shields: a) side view and b) bottom view with radiation shields above.

Variable emissivity becomes a problem because of the effect of reflected and incident radiation. Incident radiation is energy from outside sources that can be reflected off the surface being measured. This radiation reflects the temperature of the original surface it emanated from, not the surface being imaged. Fortunately, the amount of incident radiation that is reflected (or reflectivity) is based on the emissivity itself. It is a typical assumption that the emissivity ε is equal to the absorptivity α of the material [13]:

$$\varepsilon = \alpha \tag{2}$$

Also applicable is the relationship between reflectivity ρ, transmissivity τ, and absorptivity α [13]:

$$\rho + \tau + \alpha = 1 \tag{3}$$

If the surfaces are opaque, transmissivity becomes zero, and the relationship between emissivity and reflectivity becomes

$$\rho + \varepsilon = 1 \tag{4}$$

This shows that when emissivity is low, the reflectivity is high. When lower emissivity surfaces are measured, the amount of reflected radiation makes up a much larger portion of the amount of total radiation received by the camera, which skews the image. Figure 3 shows two examples of the effects of reflected radiation: one of a polished metal surface (low emissivity) that reflects the camera's own heat signature (Fig. 3a) and another of a partially painted surface with bare metal rivets that show a significantly higher temperature (Fig. 3b). In these cases, unheated surfaces that are in actuality at a uniform constant temperature exhibit hot or cold spots that are caused by the reflected radiation rather than a variation in the actual surface temperature.

Although it may appear to be a rather simple procedure to account for superfluous incident radiation in the image, the situation can be quickly compounded if there is significant temperature variation in the ambient environment. Although the camera's onboard software has the ability to account for uniform reflected radiation, it has no mechanism to account for variations in this parameter. Reflected radiation can be difficult to treat because to properly quantify it one must know the temperature of origin for each point that is reflected. In an open space, this can prove quite difficult, especially if there are numerous items or areas in the room with different temperatures. Shown in Fig. 4, the shroud is intended to block as much nonuniform reflected radiation from outside sources by surrounding the area between the camera lens and the sample being tested. Hence, the only reflected radiation will presumably be from the shroud itself, which can be maintained at a prescribed temperature. In addition, keeping the shroud at an elevated temperature is beneficial because it allows the IR camera to more easily discern the difference between the incident and emitted radiation. This discerning ability is important if the surface emissivity is to be calculated from the unheated image. If the shroud were at approximately the same temperature as the surface, it would be essentially impossible to uniquely calculate the emissivity. The heating coil wrapped around the shroud is designed to raise the temperature 20–30°C above room temperature.

Although a shroud can be successful at obstructing the outside radiation that would reflect off the material surface, the image can still be marred by the camera's own reflection off the surface. To remove the nonuniform heat signature of the camera from the images, the camera must be oriented such that the radiation emitted from the camera housing has no clear path to return to the camera's lens as reflected radiation. Images were taken at 5 deg increments from normal to the captured surface until the camera's heat signature was no longer visible. In this case, the shroud and camera are tilted at 27 deg relative to the normal of the surface being measured to eliminate this effect.

The procedure for checking for defects in a sheet material begins with placing the sample in the apparatus in which it is only contacted

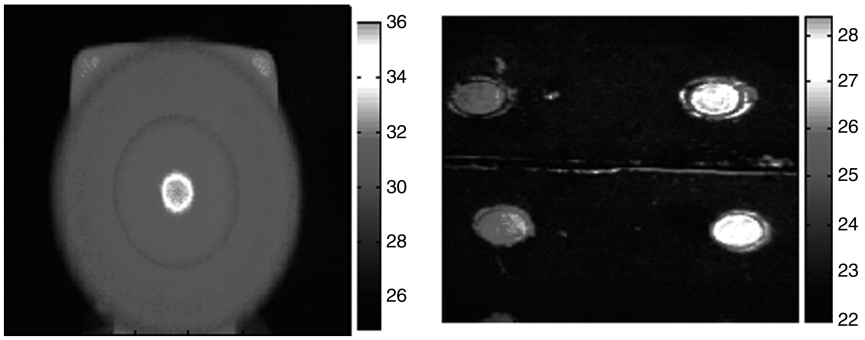

a) b)

Fig. 3 Examples of reflected radiation: a) reflection of camera's heat profile in constant temperature surface and b) image of bare rivets on the isothermal painted surface and temperature differences caused by emissivity variation.

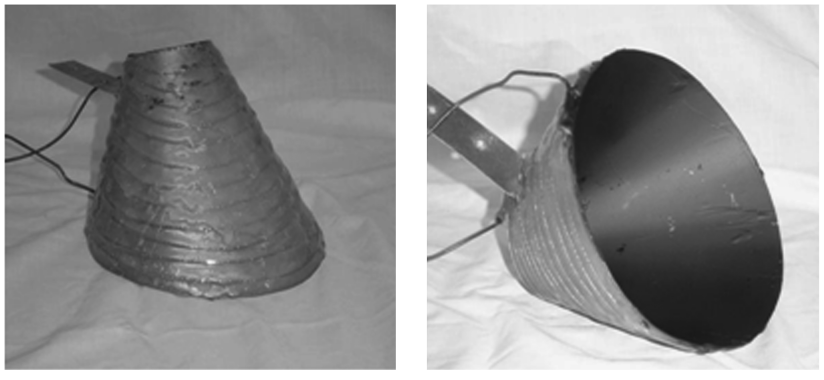

a) b)

Fig. 4 Camera shroud: a) top view of the camera shroud with the heating coil visible and b) bottom view of the camera shroud with the dark coating visible.

in a few small areas. This makes sure that little or no heat transfer occurs between the part and the holding apparatus. For each sample, the ultimate goal is a corrected thermal image that shows any defect for which the temperature gradient is unusually high. To this end, it is necessary to acquire not only the raw temperature image, but also a cold image for which the temperature is uniform and at ambient conditions. This image, captured first, will be used to calculate the emissivity of the surface, which will in turn be used to correct the image that is actively heated.

In preparation for the two-step scanning process (first a cold, or unheated, image is captured followed by a heated gradient image), the heating lamp is placed over one edge of the part with the radiation shielding as close to the part as possible. The portion of the image nearest the radiation shielding will be the top (in terms of the camera view), and the shroud will be as close to the material without touching to prevent stray radiation from skewing the data. Once both the heating lamp and camera/shroud assembly are in place, the LabVIEW data collection program can be activated. Initially, this program continually updates the image, but does not store any data. At this point, one can take advantage of the cropping, data-reduction, and noise-reduction options in the program to contour the program settings to their specific need.

The heating lamp is then turned on to begin sample heating. Heat begins to propagate along the material, and images can be taken at whatever time intervals are deemed necessary. Testing has shown that most samples are heated to acceptable temperatures (less than 20°C above the room temperature) after 30–60 s, depending on the size and thermophysical properties of the material. One must be cautious, however, to avoid prolonged exposure of the samples to high heat, which can damage not only the surface coating, but also the integrity of the part. Because the surface temperatures of the sample are elevated slightly above the room temperature, this can also avoid the complication caused by the temperature-dependent emissivity.

As previously stated, the infrared camera images are sometimes skewed by the effect of reflected radiation, and the temperatures shown in the images are not the temperature of the surface being measured, but are in fact the temperature of a surface simply being reflected. Although there have been physical adjustments in the hardware to minimize and accurately depict the amount of reflected radiation present in the signal, it is still necessary to remove it to obtain the true surface temperature. Our solution to this problem takes into account not only the raw image temperature, but also the camera settings that created the image (emissivity, ambient temperature, etc.). The solution is based on the principle that the amount of radiosity in the raw image can be corrected by determining the amount of reflected radiation and simply subtracting it, leaving only the emitted radiation:

$$\varepsilon_{\text{cam}}\sigma T_{\text{meas}}^4 + (1-\varepsilon_{\text{cam}})\sigma T_{\text{amb}}^4 = J_{\text{cam}} = \varepsilon_{\text{actual}}\sigma T_{\text{actual}}^4 + (1-\varepsilon_{\text{actual}})\sigma T_{\text{ref}}^4 \tag{5}$$

The preceding equation shows the differences between how the camera interprets the radiosity values as temperature (left side of the equation) and what the true interpretation is (the right). On the left, the temperature value for each pixel (T_{meas}) is calculated using the set camera values for the emissivity (ε_{cam}) and the ambient temperature T_{amb}. On the right, the temperature values for each pixel (T_{actual}) are calculated using the true emissivity at each point ($\varepsilon_{\text{actual}}$, calculated from the unheated image) and the reflected temperature T_{ref}, which represents the average temperature of all reflected radiation.

To calculate the true temperature values for a surface that is partially heated (T_{actual}), the other values in the equation must be known or at least estimated. The uncorrected temperature T_{meas} as well as the camera emissivity $\varepsilon_{\text{actual}}$ and ambient temperature T_{amb} are known, which leaves only the true emissivity $\varepsilon_{\text{actual}}$ and reflected temperature T_{ref} to be determined to correct the image. The reflected temperature can be taken as the temperature of the interior of the camera shroud, which is assumed to be uniform and constant. Therefore, the only variable left unknown is the true emissivity that can be calculated using a rearranged version of Eq. (5) to give

$$\varepsilon_{\text{actual}} = \frac{\varepsilon_{\text{cam}}T_{\text{meas}}^4 + (1-\varepsilon_{\text{cam}})T_{\text{amb}}^4 - T_{\text{ref}}^4}{T_{\text{actual}}^4 - T_{\text{ref}}^4} \tag{6}$$

As previously stated, the camera values of emissivity and ambient temperature are known, as well as reflected temperature. To calculate the actual emissivity, only the actual temperature needs to be known. For this calculation, the cold image can be used, because the surface temperature can be checked with a thermocouple or other temperature reading device and used as the actual temperature. Once all the variables are known, emissivity can be calculated for all pixels in the image. When the true emissivity is known, the heated images can be corrected, once again reforming the original equation:

$$T_{\text{actual}} = \sqrt[4]{\frac{\varepsilon_{\text{cam}}T_{\text{meas}}^4 + (1-\varepsilon_{\text{cam}})T_{\text{amb}}^4 - (1-\varepsilon_{\text{actual}})T_{\text{ref}}^4}{\varepsilon_{\text{actual}}}} \tag{7}$$

The actual temperature values for each pixel can be calculated using the camera settings and the newly found emissivity values as well as the reflected temperature of the camera shroud. One difficulty using this method is the sensitivity of measurements at or near ambient conditions. If the expected surface temperature is at or near the reflected temperature, it can cause a near-zero condition in the denominator of Eq. (7). Therefore, to use this method, the reflected temperature (in this case the temperature of the camera shroud) should be high enough to avoid this problem.

After the images have been stored, the next step is to remove the effects caused by reflected radiation if necessary. This would be necessary in cases in which the emissivity varies over the surface or is uniformly low. If it is not required, or after the removal has been performed, the next step is the final data conditioning in which noise can be removed with a variety of filters and a gradient image can be created. Finally, the gradient images can be inspected for suspect areas in which the gradient is unusually high. These areas of higher gradient are areas that need to be closely inspected on the surface itself and checked for signs of damage.

III. Software and Computer Program

As previously stated, the images captured by the camera can be misrepresentations of the actual surface temperature. The digital images have some amount of noise present, as well as errors in the form of reflected radiation that produce an incorrect temperature distribution. In addition to correcting the error in the images, it is also convenient to create options to adjust images to save memory, remove unwanted data, and create more meaningful images. Therefore, it is necessary to develop a software package that not only provides these options, but that is also simple in its construct so that personnel with limited computer knowledge can use it with ease.

The image capture program is the first step in analyzing the images produced by the camera. The LabVIEW virtual instrumentation panel is shown in Fig. 5. The program allows for adjustments to the image in terms of size and quality before data collection. The two methods available for size change are the cropping function and the data-reduction function. The cropping function, as the name suggests, is simply the ability to remove lines of data from all four sides of the image. This could be necessary due to misleading data at one edge of the camera's view (edge of a sample, an extraneous reflection, etc.) or to simply close in on a particular area of interest. The current function has the ability to remove up to 100 lines from any side if required. The data-reduction function is provided to create an opportunity to reduce the amount of data that is recorded without decreasing the image acquisition speed. The current output of the program is a text file of an array of temperature values that approaches 500 kB of data (unaltered) for each image. The amount of required data storage can quickly expand, depending on the time lapse between images. Therefore, it could be necessary to reduce the amount of data while still preserving the general image properties. The reduction of image size is performed by taking a prescribed

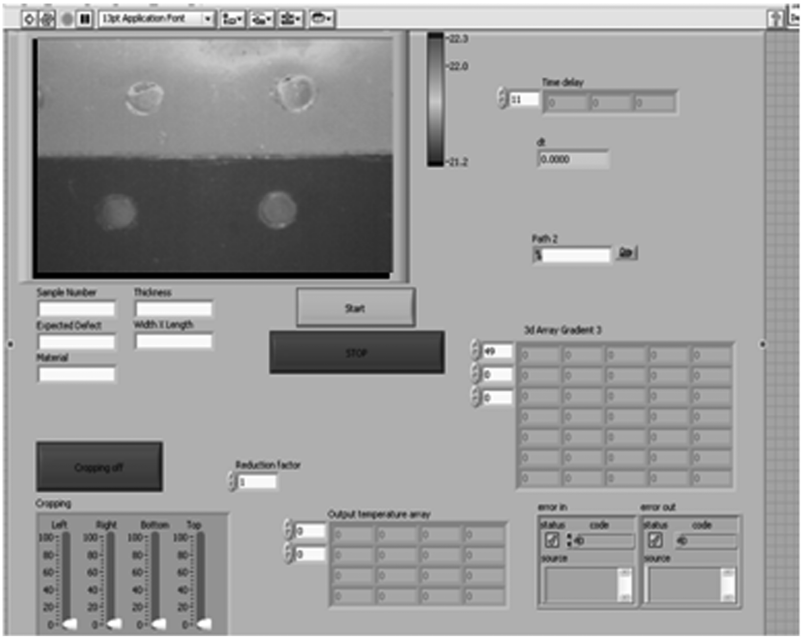

Fig. 5 Screen shot of LabVIEW image capture program.

block of pixels and averaging them (four in the case of one-half reduction, nine in the case of one-third reduction, etc.) to create a single value that is representative of the whole. In this fashion, an image's storage space can be reduced by meaningful amounts (75% in the case of one-half reduction and 89% in the case of one-third reduction). However, this can create the potential to miss smaller-sized defects due to a lower-resolution image.

After these corrections have been made, data collection can begin. First, the time delay between image captures can be adjusted to whatever duration is desired, and then the data collection can begin (and end) with the press of one button on the virtual panel. The current output of the program is a three-dimensional array that contains in each layer a complete thermographic image taken at one time step. To analyze a particular image, one must merely select a layer to retrieve it.

The Reflected Radiation Program, which was written using MATLAB, is used to extract the effects of the radiation that is initially incident on the surface. This program uses both the cold and hot images, as well as the values for emissivity and ambient temperature from the camera settings to remove the effects of reflected radiation. First, Eq. (6) is used along with the cold image to determine the emissivity map of the surface. This allows for a more detailed depiction of the amount of reflected radiation for each pixel. After the emissivity map has been created, the reflected radiation can be removed from the hot image using Eq. (7). The program produces not only the emissivity map and newly corrected heated images, but also the raw heated image, so that comparisons can be made.

Because the image produced is an electronic signal originally, it naturally contains noise that can be reduced to make the image sharper. The second program in the package, written as a MATLAB graphical user interface, is designed to filter image noise before attempting to detect thermal anomalies. The visual output of this program is shown in Fig. 6. The upper left image is the image before noise elimination, and the corrected image is in the upper right. The lower left shows the file being analyzed and the lower right image is the calculated thermal gradient. There are three options in terms of

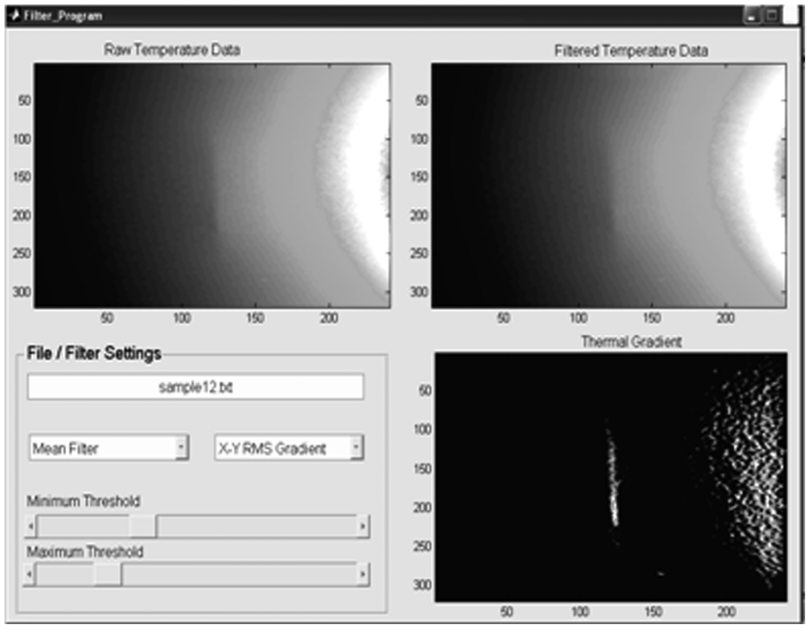

Fig. 6 Screen shot of MATLAB noise-reduction/gradient detection program.

reducing the amount of noise present in the signal: the mean filter, the median filter, and the mean gradient filter. The three options all have advantages and disadvantages in terms of removing different types of noise. The mean filter is the most simplistic of the three filters. For each pixel, as shown in Eq. (8), the filter takes the surrounding eight pixels and averages them together with the original to create a new value and does the same for all pixels in the image:

$$T_{i,j} = \left(\sum_{k=-1}^{1} \sum_{m=-1}^{1} T_{i+k,j+m} \right) \Big/ 9 \tag{8}$$

This serves to smooth the image and reduce noise, but it also has the side effect of blurring hard edges that can be potentially important.

The median filter addresses the liability of the mean filter, which is the distortion of edges and corners. This filter takes the subject pixel along with the surrounding eight pixels and sorts them from highest to lowest. After sorting, the median value is selected and used to replace the pixel being filtered. The median filter has the advantage that it does not inherently blur or damage corners and edges that appear in the image. Also, its product is all original data, whereas the mean filter is capable of producing pixel values that were not present in the original image. However, the median filter is more computationally intensive, due to the required sorting, and can slow real-time analysis.

The final filter, the mean gradient, is a newly created filter of our own design. Its design is to calculate the center point of the nine pixels selected and recalculate it based on the forward and backward differences in both the x and y directions. The differences are calculated not with the two points, but with the average of the three pixel values in the corresponding row or column:

$$T_{i,j} = T_{i+1,j} - \left[\left(\frac{1}{3} \sum_{k=-1}^{1} T_{i+1,j+k} \right) - \left(\frac{1}{3} \sum_{k=-1}^{1} T_{i,j+k} \right) \right] \tag{9}$$

$$T_{i,j} = T_{i-1,j} - \left[\left(\frac{1}{3} \sum_{k=-1}^{1} T_{i-1,j+k} \right) - \left(\frac{1}{3} \sum_{k=-1}^{1} T_{i,j+k} \right) \right] \tag{10}$$

$$T_{i,j} = T_{i,j+1} - \left[\left(\frac{1}{3} \sum_{k=-1}^{1} T_{i+k,j+1} \right) - \left(\frac{1}{3} \sum_{k=-1}^{1} T_{i+k,j} \right) \right] \tag{11}$$

$$T_{i,j} = T_{i,j-1} - \left[\left(\frac{1}{3} \sum_{k=-1}^{1} T_{i+k,j-1} \right) - \left(\frac{1}{3} \sum_{k=-1}^{1} T_{i+k,j} \right) \right] \tag{12}$$

After all four differences are calculated, four potential center pixel values are calculated, then averaged to create a new center value. Although this method is excellent for creating a filter that smoothes the data based on an accurate gradient, it favors the edge points over the corner points by a 2-to-1 margin when performing analysis.

After noise reduction, the program creates a temperature gradient image, presumably showing areas in which heat flux has slowed, creating a high gradient. Currently, there are two gradient methods available in the program: the rms gradient and the max/min gradient. The rms gradient calculates the gradient for each pixel based on the following formula:

$$G_{i,j} = \sqrt{(T_{i-1,j} - T_{i+1,j})^2 + (T_{i,j-1} - T_{i,j+1})^2} \tag{13}$$

This provides a combination of both the x and y gradients at each point. The max/min gradient is calculated by locating the maximum and minimum values within the nine pixels analyzed and subtracting the two to create the highest gradient possible. Although the rms gradient creates a more accurate account of the gradient at each point in terms of a true gradient value, the max/min will make the gradients more visible. However, the max/min gradient requires a sorting of values to detect the maximum and minimum, which is computationally intensive and can slow processing.

IV. Results and Discussion

The results contained here are an attempt to first verify the ability of the system to detect crack defects and then to test the ability of the three programs created to perform the image correction and filtering tasks. The tests selected use a variety of crack orientations and sizes as well as a selection of emissivity situations. The goal of each test is to first remove any effects of radiation and any unwanted noise and then to visually scan the images for evidence of the defects.

The sample shown in Fig. 7 was created by first using a rotary cutting tool to remove some material from the back side of the plate in the area selected for the crack. The part is then mechanically bent until a larger crack develops. The surface is then painted to hide the crack's presence. The infrared camera is then activated and two pictures are taken: one of the cold (or unheated) surface and the other of the heated surface.

Because neither image exhibits any obvious camera artifacts and the surface is well coated and of uniform emissivity, it is not necessary to process the image using the reflected radiation program; thus, only the noise-reduction/gradient program was used. The results of this test are visible in Fig. 8. Using the mean filter and X–Y rms gradient, the raw thermal image (upper left) is first filtered (upper right), then the gradient calculated (lower right). Note the large gradient spike where the crack is located.

The sample used (Fig. 9) is similar to the last one in that the surface is completely coated with paint, but the crack in this case is oriented 45 deg relative to the heat flux direction. Because the surface is uniform in coating, no alteration is needed before noise reduction and gradient calculation. Once again, as shown in Fig. 10, the crack is plainly visible after noise removal and gradient calculation. However, when compared with the previous example, one notices that this defect has a smaller thermal signature than its actual size. This is anticipated, because at an angle, the crack provides less area to block heat flow.

The sample shown in Fig. 11 was created in the same fashion as the previous one with the exceptions that the crack is now at a 45 deg angle with respect to the heat flux direction and there is an area of bare metal that was not painted. This test is to determine whether the current software can differentiate between the emissivity change and the actual defect. No cropping or data reduction is necessary for this sample, and so the first step is to attempt to remove the effects of

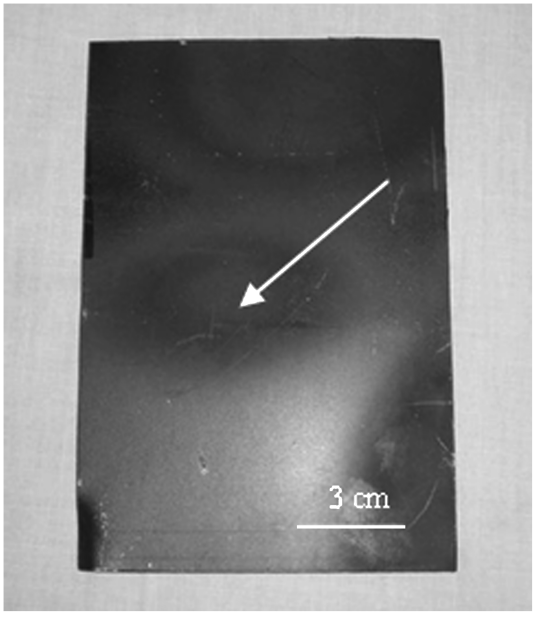

Fig. 7 Sample for test 1 (0.8-mm-thick steel painted black with a longitudinal crack 3.5 cm in length).

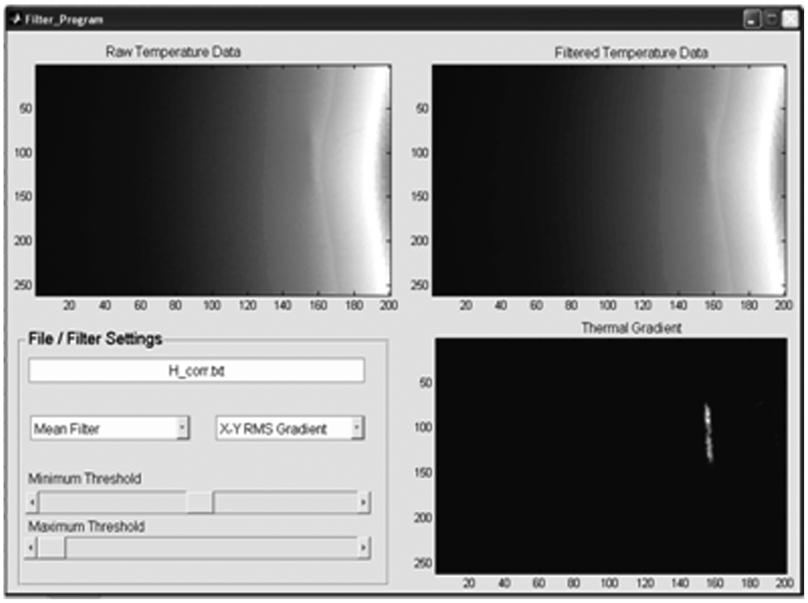

Fig. 8 Screen shot of noise reduction and gradient calculation for test 1.

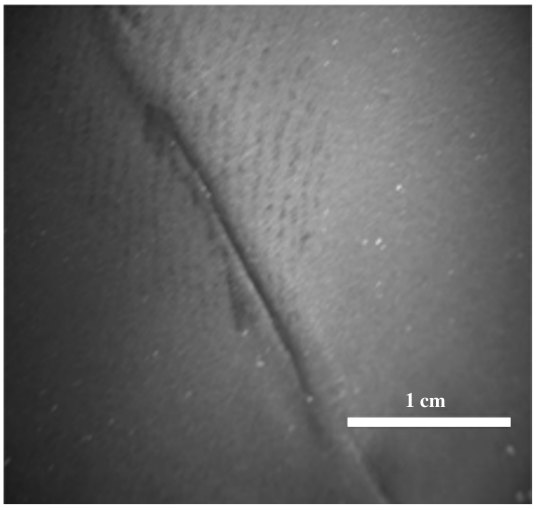

Fig. 9 Sample for test 2 (0.8-mm-thick steel with an angled crack approximately 5 cm in length).

reflected radiation. The first product of the program is to calculate the true emissivity of the surface, which can be seen in Fig. 12. The emissivity of the sample exhibits values that correspond well with the types of surface finishes visible on the part, with the painted areas at approximately 0.9 and the unpainted surfaces at an emissivity of approximately 0.5. One area of concern is the upper right corner, where the emissivity appears to be slightly above 1. This is presumably because one corner of the camera shroud was visible in the image.

Figure 13 shows that the correction for the heated image is only a slight improvement over the original one. Although the low-

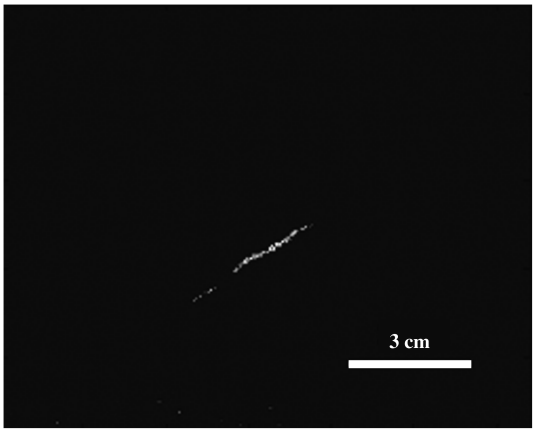

Fig. 10 Gradient image for sample 2.

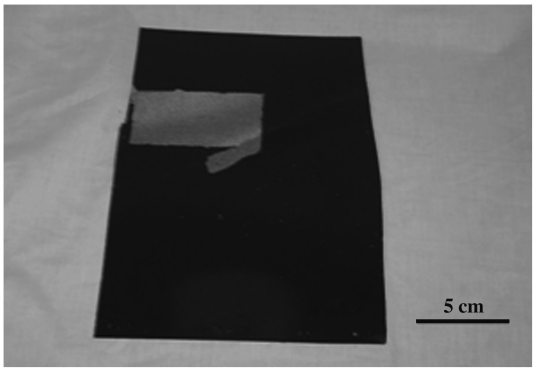

Fig. 11 Sample for test 3 (0.8-mm-thick steel with a 45 deg crack across the unpainted portion of sample).

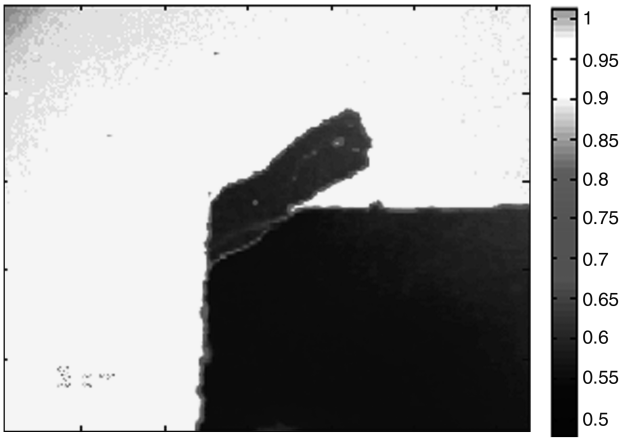

Fig. 12 Emissivity map of sample 3. The dark area is the area that is bare metal (low emissivity), and the rest is painted (high emissivity).

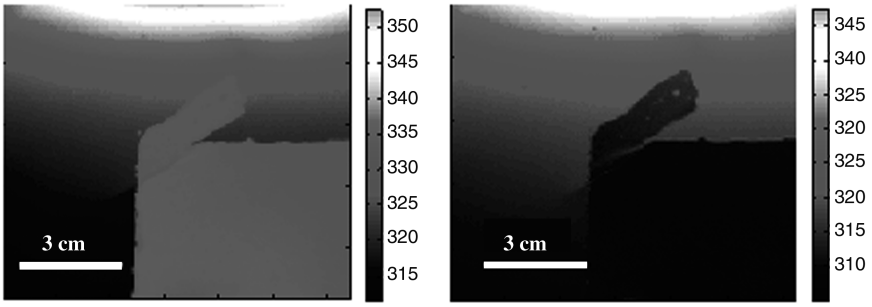

a) b)

Fig. 13 Heated images of sample 3: a) raw temperature image and b) corrected temperature image (temperature in Kelvin).

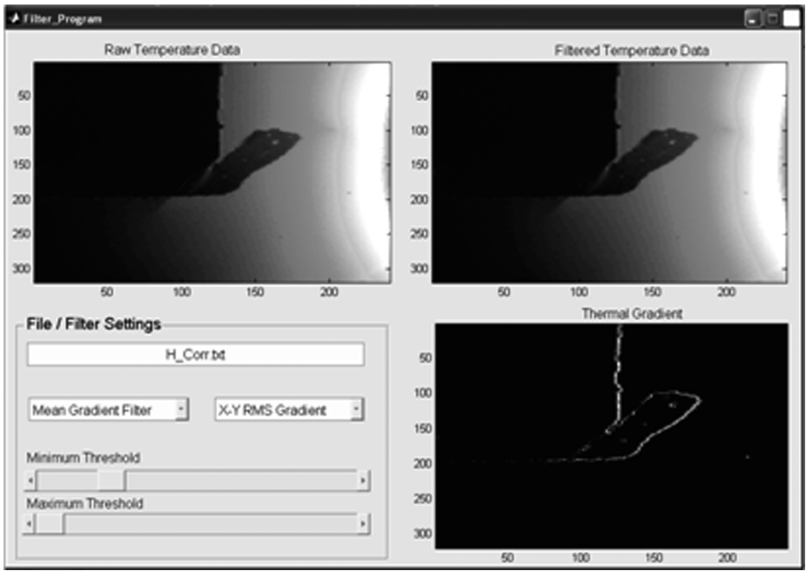

Fig. 14 Screen shot of noise-reduction/gradient program for sample 3.

emissivity region is closer to the surrounding temperature in the corrected image, the entire image has shown a decrease in temperature, even in the areas in which it is assumed that a correct temperature is seen in the original. Noise reduction and gradient calculations of every type and combination are unsuccessful in this case, as can be seen in Fig. 14, in which the gradient image shows not only the crack defect, but also the barrier between painted and bare metal surfaces. This makes the crack difficult to distinguish among the other spikes in gradient. Therefore, it is unlikely in this case that a defect could be identified without prior knowledge.

V. Conclusions

The current system proved successful at detecting defects in coated surfaces, in which the emissivity is high. The scanning system has proven adept at detecting cracks not only at optimal angles of detection, but also at less than desirable angles. Although most tests in this case were of steel samples, changes in materials will affect the rate of heat transfer through the material, which in turn affect the rate of thermal signal propagation. The system could presumably be used for nonmetals with adjustments to the operating temperature of the heating element. The scanning system has also proven successful at detecting small cracks to a size of slightly under 1 cm. It is not unreasonable to believe that detection of even smaller defects can be achieved by decreasing the distance between the camera and the surface, thereby making the view area smaller.

The current attempts to scan surfaces with variable emissivity have been only marginally successful. In cases in which the emissivity range is limited, the images fare better after correction, but when the emissivity range is large, remnants of reflected radiation remain and make it difficult to not only get an accurate surface temperature map, but also to locate defects within the material. Possibilities for these difficulties could be a lack of uniformity of reflected temperature, a change in scattering between areas of emissivity change, and the heat transfer alterations caused by coating the surfaces.

There are several possibilities for continued research and improvement of this system. First, as previously mentioned, the three programs currently used for analysis can be combined into one program that can handle all analysis procedures. Additional research can be done to see how the system performs when detecting defects of other varieties, including delamination, corrosion, pinholes, etc. The physical system can be changed to allow for easier adjustment of height, as well as a larger area for materials. The camera shroud's current configuration can be improved to create a more uniform temperature along its surface, which in turn will assist in reflected radiation calculations. All current results have been with the camera motionless; to create a true scanning system, automated position sensing must be added to allow the system to translate horizontally as images are taken as well to as record the distance traveled.

Finally, although there has been some success at accounting for the effects of reflected radiation, further testing must be done to improve the quality of the corrected images. This includes not only better uniformity of the reflected temperature, but also improving the equations and algorithms.

References

[1] Mix, P. E., *Introduction to Nondestructive Testing: A Training Guide*, 2nd ed., Wiley, New York, 2005.

[2] Maldague, X. P. V., *Theory and Practice of Infrared Technology for Nondestructive Testing*, Wiley, New York, 2001.

[3] Penner, N., *Non-Destructive Thermal Imaging of Metal Samples*, Undergraduate Research Final Report, Univ. of Oklahoma, Norman, OK, 2007.

[4] Sayers, C. M., "Detectability of Defects by Thermal Non-Destructive Testing," *British Journal of Non-Destructive Testing*, Vol. 26, No. 1, 1984, pp. 28–33.

[5] Killey, A., and Sargent, J. P., "Analysis of Thermal Non-Destructive Testing," *Journal of Physics D: Applied Physics*, Vol. 22, No. 1, 1989 pp. 216–224.
doi:10.1088/0022-3727/22/1/032

[6] Cramer, K. E., Winfree, W. P., Howell, P. A., Syed, H. I., and Renouard, K. A., "Thermographic Imaging of Cracks in Thin Metal Sheets," *Proceedings of SPIE: The International Society for Optical Engineering*, Vol. 1682, 1992, pp. 162–170.
doi:10.1117/12.58532

[7] Cramer, K. E., "Quantitative Thermal Imaging of Aircraft Structures," *Proceedings of SPIE: The International Society for Optical Engineering*, Vol. 2473, 1995, pp. 226–232.
doi:10.1117/12.204859

[8] Cramer, K. E., and Winfree, W. P., "Thermal Characterization of Defects in Aircraft Structures via Spatially Controlled Heat Application," *Proceedings of SPIE: The International Society for Optical Engineering*, Vol. 2766, 1996, pp. 202–209.
doi:10.1117/12.235376

[9] Cramer, K. E., and Winfree, W. P., "Thermographic Imaging of Material Loss in Boiler Water-Wall Tubing by Application of Scanning Line Source," *Proceedings of SPIE: The International Society for Optical Engineering*, Vol. 3995, 2000, pp. 600–609.
doi:10.1117/12.387854

[10] Cramer, K. E., and Winfree, W. P., "Application of the Thermal Line Scanner to Quantify Material Loss Due to Corrosion," *Proceedings of SPIE: The International Society for Optical Engineering*, Vol. 4020, 2000, pp. 210–219.
doi:10.1117/12.381553

[11] Woolward, D. F., and Cramer, K. E., "Line Scan versus Flash Thermography: Comparative Study on Reinforced Carbon-Carbon," *Proceedings of SPIE: The International Society for Optical Engineering*, Vol. 5782, 2005, pp. 315–323.
doi:10.1117/12.603789

[12] ThermoVision A20M Operator's Manual, 2007.

[13] Dewitt, D. P., and Incropera, F. P., *Fundamentals of Heat and Mass Transfer*, 5th ed., Wiley, New York, 2001.